

Plasmonic Bidirectional/Unidirectional Wavelength Splitter Based on Metal-Dielectric-Metal Waveguides

Kunhua Wen¹ · Yihua Hu¹ · Li Chen¹ · Jinyun Zhou¹ · Liang Lei¹ · Ziming Meng¹

Received: 3 April 2015 / Accepted: 30 June 2015 / Published online: 15 July 2015
© Springer Science+Business Media New York 2015

Abstract A plasmonic bidirectional/unidirectional wavelength splitter based on asymmetric metal-dielectric-metal (MDM) waveguides is proposed. In the splitter, owing to the interference effects caused by the unequal phase delays from the two asymmetric arms of MDM waveguides, surface plasmon polaritons (SPPs) will only transmit through the output port that is close to the arm where constructive interference arises. The transmission wavelengths can be linearly modulated by changing the lengths of the arms. Since two different SPP modes are obtained in two output ports, respectively, the structure can act as a bidirectional wavelength splitter. Interestingly, both SPP modes can be manipulated to transmit through the same port by adding a notch in one arm. In this case, the notch must simultaneously locate at the anti-node and at the node of the magnetic fields of two SPP modes respectively. As a result, additional phase delay for the specific mode will be produced by the notch, but without any impact on the other mode. Then, the propagation directions of both modes will turn to be identical. High transmission and high cross-talk isolation are investigated for all the cases by using the finite-difference time-domain method.

Keywords Plasmonic · Wavelength splitter · Metal-dielectric-metal (MDM) waveguide

Introduction

In view of the development of integrated photonics, various approaches have been proposed to design micro-nano optical components or systems, such as silicon-based waveguides, photonic crystal, plasmonic waveguides, and so on [1–4]. Among these technologies, it is worthy to point out that the future development of all optical communications and highly integrated photonic circuits may benefit from the research of surface plasmon polaritons (SPPs), which can overcome the classical optical diffraction limits. Particularly, plasmonic metal-dielectric-metal (MDM) waveguides have attracted considerable interest because of their advantages of strong confinement of SPPs, low propagation loss, and simple manufacture process. Thus, numerous MDM-based devices have been developed, including optical switches, Mach-Zehnder interferometers, biomedical sensors, wavelength filters, and so on [5–17]. In an integrated optical circuit, it is quite necessary to control the SPP propagation direction or split SPPs into multiple output waveguides with expected wavelengths or power ratios. For example, SPPs at different wavelengths could travel in the desired directions by setting different notches or cavity resonators on the opposite sides of an MDM waveguide. Y-shaped MDM waveguides were also employed to split SPPs into its two arms [18, 19]. Besides, unidirectional excitation of SPPs was achieved by the interference effects at the exits of multiple slits [20–24]. Recently, directional SPP propagation and coupling phenomena were also demonstrated through the polarization-sensitive apertures in a gold film and the near-field interference effects of a circularly polarized light, respectively [25, 26]. However, the performances, such as the transmissions, cross-talk isolations, wavelength manipulation, etc., are not satisfactory enough to favorably compare with that of the classical fiber equipments.

✉ Kunhua Wen
khwen@gdut.edu.cn; wkh2003@gmail.com

¹ School of Physics and Optoelectronic Engineering, Guangdong University of Technology, Guangzhou 510006, Guangdong, China

In this paper, a high-performance subwavelength MDM splitter is proposed by using an asymmetric rectangular waveguide. As SPPs at the exits of the arms are contributed from two optical paths with unequal widths, interferences will arise due to the different phase delays. SPPs at the desired wavelengths will transmit through Port1 or Port2 close to the arm where constructive interference occurs, and high cross-talk isolations will be simultaneously obtained at Port2 or Port1, respectively. Besides, by adding a notch in the arm to modulate the phase delay, the propagation directions for both SPP modes can be changed to be identical. The performances of the structure are investigated through the finite-difference time-domain (FDTD) method with perfectly matched layer (PML) boundary conditions. The results show that favorable performances are available for all the cases. As both SPP modes will separately propagate through two ports or they will simultaneously transmit towards only one port, the device can serve as a bidirectional/unidirectional wavelength splitter.

Bidirectional Wavelength Splitter

The proposed wavelength splitter is shown in Fig. 1. The metal and dielectric are assumed to be silver and air, respectively. An MDM bus waveguide is connected to an asymmetric rectangular structure, which provides two output ports in opposite directions. According to the dispersion equation of TM mode, the effective refractive index n_{eff} will be significantly affected by the width of the waveguide. Therefore, the width of two arms (named as Arm1 and Arm2) are set to be different as W and D to obtain different phase delays. Usually, the effective refractive index n_{eff} of the MDM structure can be obtained through [27]

$$\varepsilon_i k_m + \varepsilon_m k_i \tanh(-jk_i d/2) = 0 \quad (1)$$

$$n_{\text{eff}} = \beta/k_0 \quad (2)$$

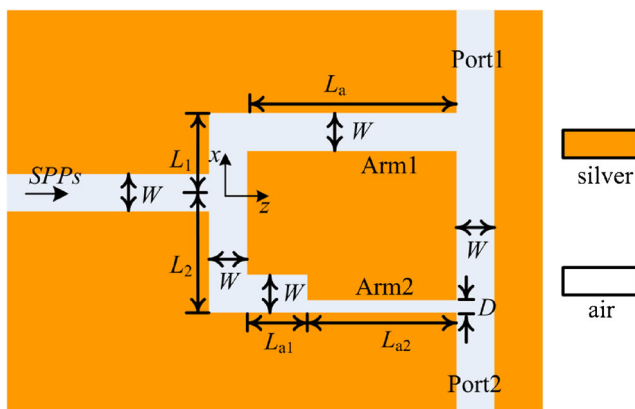


Fig. 1 Scheme of bidirectional wavelength splitter

where $k_0 = 2\pi/\lambda$ and β are the wave numbers of light in vacuum and waveguide, respectively, $k_{i,m} = \sqrt{\varepsilon_{i,m} k_0^2 - \beta^2}$ is the transverse propagation constant in air and silver, respectively, d is the general definition of the waveguide width (W or D can be substituted for it), and ε_i and ε_m are the dielectric constants of air and silver, respectively.

After launching into the bus waveguide, SPPs will be separated into two parts at the intersection of the asymmetric rectangular structure and then propagate along its two arms, respectively. To make the bidirectional SPP splitting available, one should guarantee that destructive interferences and constructive interferences of SPPs at the desired wavelengths must occur at the exits of the two arms, respectively. For example, SPPs at the exit of Arm2 are contributed from two parts, one of which propagates along Arm1 and then through the middle output waveguide and the other from Arm2 directly. When the matched output port for SPPs at λ_1 is assumed to be Port1, constructive interference and destructive interference must arise at the exit of Arm1 and Arm2, respectively. As such, a high transmission for Port1 and a high cross-talk isolation for Port2 are obtained synchronously. In this case, the phase delays must satisfy the condition:

$$\theta_2 + n_w L \frac{2\pi}{\lambda_1} = \theta_1 + 2N\pi \quad (3)$$

$$\theta_1 + n_w L \frac{2\pi}{\lambda_1} = \theta_2 + (2M + 1)\pi \quad (4)$$

where $\theta_1 = (L_1 + L_a)2\pi n_w/\lambda_1 + \phi_0$ and $\theta_2 = (L_2 + L_{a1})2\pi n_w/\lambda_1 + 2\pi n_s L_{a2}/\lambda_1$ are the phases at the exits of Arm1 and Arm2, respectively, ϕ_0 denotes the initial phase difference between the directly generated up-going and down-going SPPs by the bus waveguide, $n_{w,s}$ are the real parts of the effective indices of Arm1 and Arm2, $L = L_1 + L_2$ is the total length of the vertical side of the rectangular structure, $L_1, 2$ are the corresponding lengths of upper and lower parts, $L_{a1}, a2$ are the lengths of two parts of Arm2, L_a is the total length of an arm, and N and M are integers.

According to Eqs. (3) and (4), the following phase condition can be obtained:

$$\begin{aligned} \theta_1 - \theta_2 &= \frac{2\pi}{\lambda_1} [(L_1 - L_2)n_w + (n_w - n_s)L_{a2}] + \phi_0 \\ &= K\pi + \frac{\pi}{2} \end{aligned} \quad (5)$$

where K is a positive or negative integer. When Eqs. (3)–(5) are achieved, SPPs at λ_1 will only propagate towards Port1. Likewise, when the phase conditions of SPPs at λ_2 are reversed at the exits of Arm1 and Arm2, the matched output port for λ_2 turns to be Port2. Specifically, Eqs. (3) and (4) should be rewritten as $\theta'_1 + n_w L \frac{2\pi}{\lambda_2} = \theta'_2 + 2N\pi + \phi'_0$ and $\theta'_2 + n_w L \frac{2\pi}{\lambda_2} = \theta'_1 + (2M + 1)\pi$, respectively. Obviously, the supported transmission wavelengths for two output ports are

different, and thus, the proposed structure can serve as a bidirectional wavelength splitter.

In the following, the FDTD method with PML boundary conditions is employed to investigate the performances of the structure. PML layers with reflection of 0.0001 are set to surround the whole structure, and the grid sizes along x - and y -directions are chosen to be $\Delta x = \Delta y = 5$ nm. The fundamental TM mode of the plasmonic waveguide is excited by a plane wave incident from the input waveguide. Two monitors are placed in Port1 and Port2 to obtain the transmission. By comparing the transmittances in two output ports, we can directly obtain the isolation at the specific wavelength. Other parameters are specified as follows: the width of Arm2 is $D = 20$ nm, the widths of all other waveguides are defined as $W = 60$ nm, the lengths of two parts of the structure's left side are $L_1 = 155$ nm and $L_2 = 305$ nm, and the beginning length of Arm2 is $L_{a1} = 100$ nm. In addition, the detailed values of the optical constant of silver [28] are used during the simulations. The simulated spectra are shown in Fig. 2, where the length of the right side of Arm2 is considered as $L_{a2} = 400$ nm or $L_{a2} = 450$ nm, respectively. Detailed results, including the wavelengths and the transmissions, are shown in Table 1. By taking $\lambda_2 = 1412.2$ nm and $L_{a2} = 400$ nm for example, we can obtain $n_w = 1.298$ and $n_s = 1.713$ through Eqs. (1) and (2). Furthermore, $\theta_2 - \theta_1 \approx 0.51\pi$, which generally agrees with the analysis result, is obtained according to Eq. (5).

Obviously, the supported transmission wavelengths for two output ports are demonstrated to be completely different. A high transmittance will be achieved for the matched output waveguide while a high cross-talk isolation will be available for the other port in its opposite direction.

To analyze the electromagnetic responses of the structure, the magnetic fields for SPPs at the transmission wavelengths that correspond to the ones in Fig. 2 are provided in Fig. 3. In

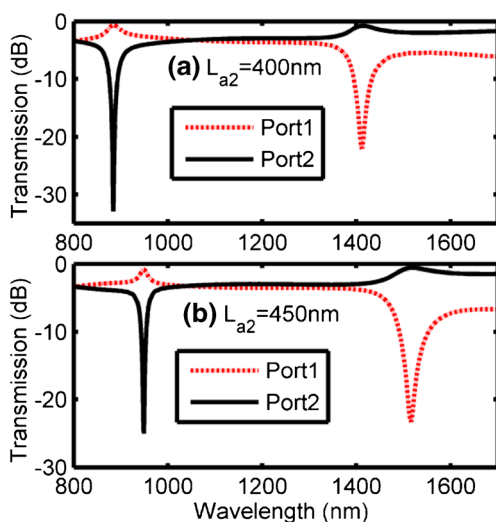


Fig. 2 Transmission spectra for Port1 and Port2 with **a** $L_{a2} = 400$ nm and **b** $L_{a2} = 450$ nm

Table 1 Simulation results with different L_{a2}

| L_{a2} (nm) | λ_1 (nm) | Transmission (dB) | | λ_2 (nm) | Transmission (dB) | |
|---------------|------------------|-------------------|-------|------------------|-------------------|-------|
| | | Port1 | Port2 | | Port1 | Port2 |
| 400 | 883.8 | -0.6 | -32.9 | 1412.2 | -22.0 | -0.8 |
| 450 | 948.2 | -0.9 | -25.0 | 1515.6 | -23.2 | -0.6 |

the rectangular circle, there is a slight resonance effect that is analogous to the ring cavity effect. However, since both sides of the circle are connected to the input and output waveguides directly, thus, the resonance effect will be weaker than those ring cavity filters, which have a coupling distance to the bus waveguide. Moreover, by taking Fig. 3a for example, the matched output port for SPPs at 883.8 nm should be Port1 based on the above transmission spectrum. It can be found that constructive interference and destructive interference occur at the exits of Arm1 and Arm2 in Fig. 3a, respectively. Therefore, most of the SPP energy directly passes through Port1, and there are almost no SPPs distributed in the output waveguide towards Port2. On the contrary, the propagation status for SPPs at 1412.2 nm is completely different in Fig. 3b, which shows that SPPs only transmit through Port2. These results are highly in accordance with that presented in Fig. 2a. Moreover, the magnetic fields of SPP modes at 948.2 and 1515.6 nm of

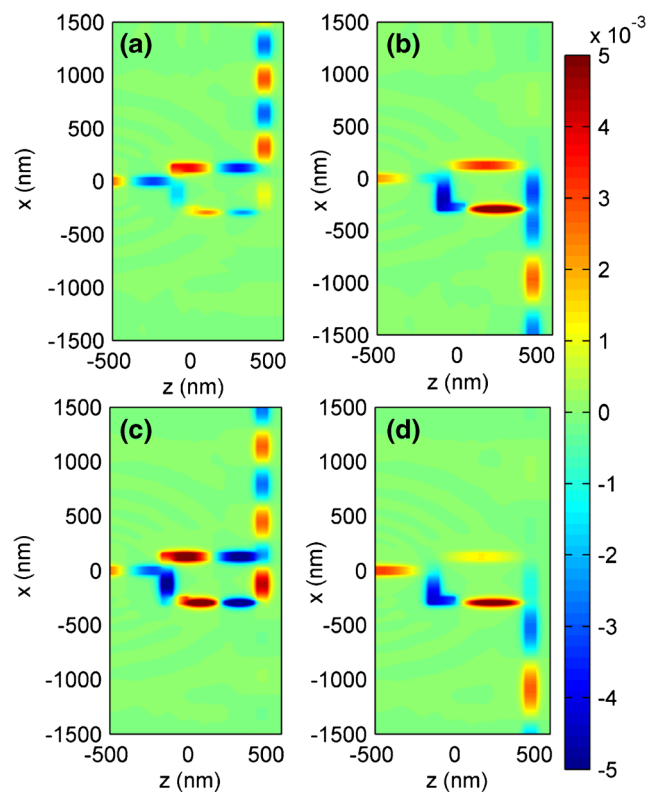


Fig. 3 The magnetic fields for SPPs at the transmission wavelengths corresponding to that in Fig. 2: **a** 883.8 nm, **b** 1412.2 nm, **c** 948.2 nm, **d** 1515.6 nm

Fig. 2b are also shown in Fig. 3c, d, which demonstrate that SPPs propagate only towards Port1 and Port2, respectively.

Being compared with the results in Fig. 2a, b, a red shift phenomenon for the transmission wavelengths will arise at both ports by increasing L_{a2} . To find out more details, L_{a2} is increased from 400 to 500 nm with a step of 10 nm while other parameters are fixed. The simulation results are shown in Fig. 4. The wavelength increase steps for Port1 and Port2 are fixed as about 18.6 and 11.8 nm, respectively, and thus, a linear relationship between the transmission wavelength and L_{a2} is confirmed. The simulated result agrees well with the theory analysis in Eq. (5), which indicates a linear influence of L_{a2} on the wavelength. Actually, the working frequency of our proposed structure can cover the range from visible light to infrared light that supports the SPPs generation, provided that the phase conditions are matched to Eqs. (3) and (4). This character may offer great flexibility to design the structure and one can easily obtain the desired transmission wavelength for the expected output port.

Besides, the left side of the rectangular structure is also lengthened, while other parameters are the same as that in Fig. 2b. We can obtain the length differences of $\Delta L=L_2-L_1=70, 90, 110$ nm, as $L_1=165, 175, 185$ nm and $L_2=335, 365, 395$ nm are defined in Fig. 5a–c, respectively. According to Eq. (5), the length differences of ΔL will also affect the transmission wavelength linearly, which is further confirmed by the simulated transmission spectra in Fig. 5. The detailed results are shown in Table 2. Obviously, both the SPP mode at λ_1 for Port1 and the mode at λ_2 for Port2 increase linearly with ΔL . Besides, it can be found that the cross-talk isolation for the unmatched output port receives a little tolerable penalty by increasing ΔL , but we still consider that the structure can successfully serve as a bidirectional wavelength splitter. More details about the magnetic field distributions can be seen in the insets of Fig. 5.

Unidirectional Wavelength Splitter

Based on the above analyses and simulations, it can be understood that the transmission wavelengths can be manipulated

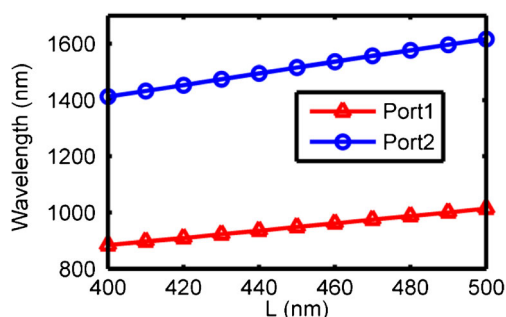


Fig. 4 The transmission wavelength variation with respect to L_{a2}

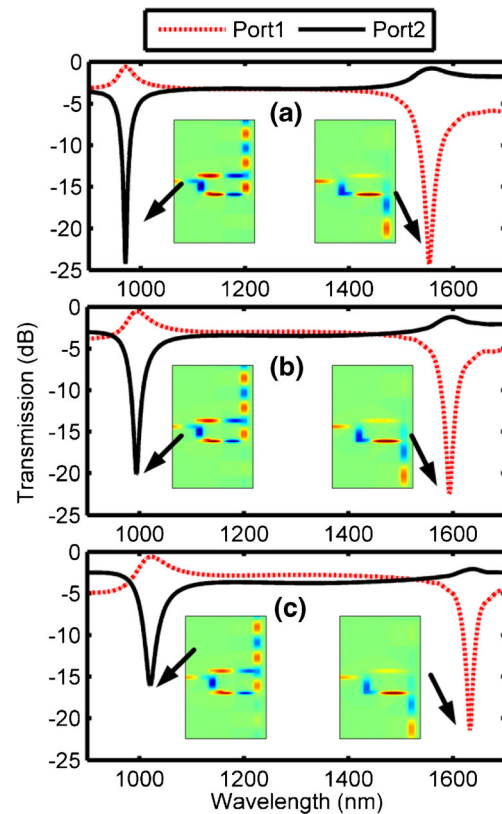


Fig. 5 Transmission spectra for Port1 and Port2 with a $L_1=165$ nm, $L_2=335$ nm, b $L_1=175$ nm, $L_2=365$ nm, and c $L_1=185$ nm, $L_2=395$ nm

by changing ΔL or L_{a2} . However, the propagation directions for both modes are separated to two opposite sides in this structure. It is interesting to point out that unidirectional propagation for all the modes may be desired in the integrated photonic circuits. In this case, one should change the phase delay of one optical path to guarantee that destructive interferences for both modes will occur at the exit of Arm1 or Arm2 simultaneously.

On the basis of the scheme in Fig. 1, a notch is added in Arm1 to modulate the phase delay, as shown in Fig. 6. Note that the position of the notch, which is denoted by D_s , is a significant factor to obtain the unidirectional propagation for both modes. Specifically, in Fig. 2, the matched output ports for SPP modes at λ_1 and λ_2 are Port1 and Port2, respectively. If both modes are expected to transmit through Port1 only, the notch must locate at the node of magnetic field of λ_1 (i.e.,

Table 2 Simulation results with different L_1 and L_2

| L_1, L_2 (nm) | λ_1 (nm) | Transmission (dB) | | λ_2 (nm) | Transmission (dB) | |
|-----------------|------------------|-------------------|-------|------------------|-------------------|-------|
| | | Port1 | Port2 | | Port1 | Port2 |
| 165, 335 | 970.2 | -0.6 | -24.2 | 1554.7 | -24.3 | -0.8 |
| 175, 365 | 994.2 | -0.5 | -20.1 | 1592.5 | -22.3 | -1.2 |
| 185, 395 | 1020.5 | -0.6 | -16.0 | 1632.0 | -21.4 | -2.1 |

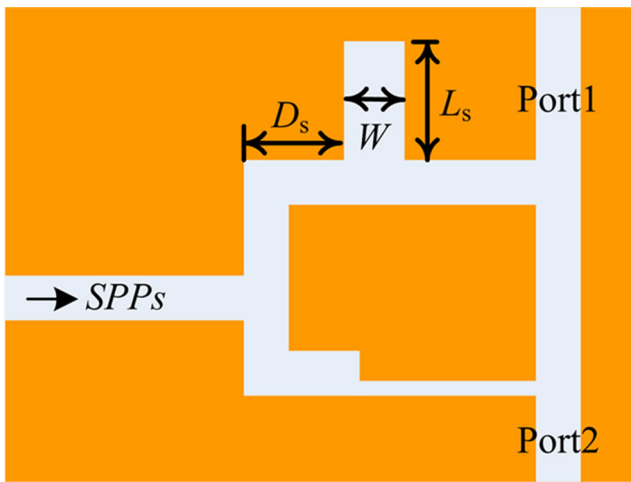


Fig. 6 Scheme of unidirectional propagation for both modes

$|H_y|=0$) and at the anti-node of λ_2 (i.e., $|H_y|=\text{Max}$) simultaneously. In this case, SPPs at λ_1 will pass the notch directly without additional phase delay. However, SPPs at λ_2 will be captured into the notch, and thus, the phase delay is modulated. By properly designing the length of the notch, destructive interferences and constructive interferences for both modes are achieved at the exits of Arm2 and Arm1, respectively. In this case, the phase delays of SPP modes at λ_1 and λ_2 will together obey Eqs. (3) and (4). Besides, Eq. (5) is still suitable for the mode at λ_1 but should be rewritten for the mode at λ_2 as

$$\begin{aligned} \theta_2 - \theta_1 &= \frac{2\pi}{\lambda_2} [(L_2 - L_1)n_w + (n_s - n_w)L_{a2} - 2L_s n_w] + \phi_0 + \varphi \\ &= K\pi + \frac{\pi}{2} \end{aligned} \tag{6}$$

where L_s is the length of the notch and φ is the phase delay caused by the reflection on the end of the notch. Then, SPPs at λ_1 and λ_2 will only propagate towards Port1. Interestingly,

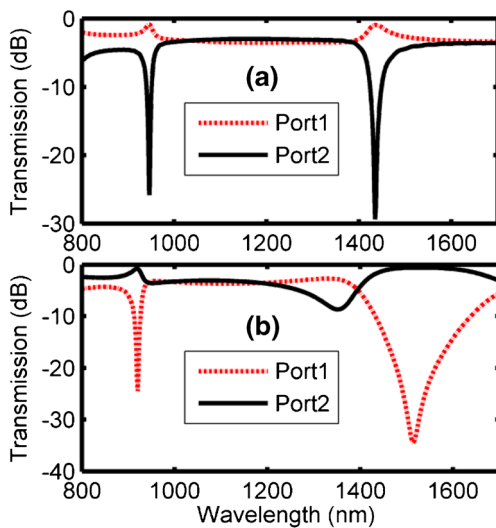


Fig. 7 Transmission spectra for Port1 and Port2 with **a** $D_s=305$ nm and $L_s=365$ nm and **b** $D_s=0$ nm and $L_s=220$ nm

Table 3 Simulation results with different D_s and L_s

| D_s, L_s (nm) | λ_1 (nm) | Transmission (dB) | | λ_2 (nm) | Transmission (dB) | |
|-----------------|------------------|-------------------|-------|------------------|-------------------|-------|
| | | Port1 | Port2 | | Port1 | Port2 |
| 305, 365 | 945.9 | -0.9 | -25.9 | 1435.0 | -0.9 | -29.4 |
| 0, 220 | 919.9 | -24.5 | -0.8 | 1514.1 | -34.4 | -0.5 |

when the notch locates at the anti-node of H_y of λ_1 and at the node of λ_2 simultaneously, the matched output ports for both SPPs modes turn to be Port2.

In the following simulation, the width of the notch is $W=60$ nm and other parameters are the same as that in Fig. 2b. The transmission spectra are shown in Fig. 7a with $D_s=305$ nm and $L_s=365$ nm and in Fig. 7b with $D_s=0$ nm and $L_s=220$ nm. Obviously, the matched output ports for both SPP modes are Port1 or Port2 in Fig. 7a, b, respectively. The detailed results are shown in Table 3. High transmission for the matched output port and high cross-talk isolation for the other port are also achieved for both modes.

The magnetic field distributions in Fig. 8a, b correspond to the transmission wavelengths in Fig. 7a, while the ones in Fig. 8c, d correspond to the transmission wavelengths in Fig. 7b. For example, it can be seen that most of the SPPs at 945.9 nm directly pass through the notch in Fig. 8a as the

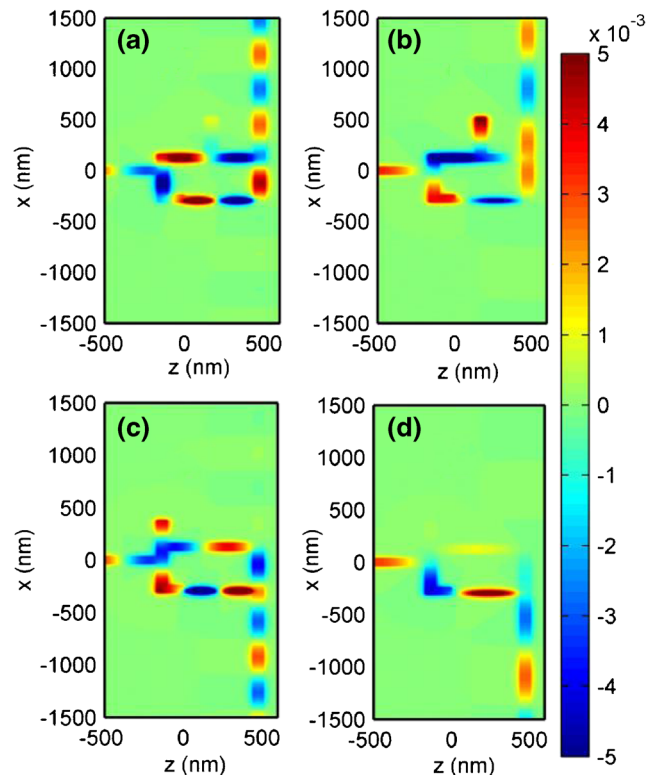


Fig. 8 The magnetic fields for SPPs at the transmission wavelengths corresponding to those in Fig. 7: **a** 945.9 nm, **b** 1435.0 nm, **c** 919.9 nm, and **d** 1514.1 nm

notch locates at the node of H_y . However, different situations arise for SPPs at 1435.0 nm in Fig. 8b, where SPPs are captured into the notch for the reason that the magnetic field reaches almost the maximum value at the position of the notch. According to the interference effects at the exits of the arms, SPPs at both wavelengths only transmit through Port1. Moreover, the output ports for both modes are Port2 only in Fig. 8c, d because the SPP distributions in the notch are opposite to that in Fig. 8a, b, respectively. As SPPs at all the desired wavelengths will transmit only through the matched port in one direction, the proposed structure can act as a unidirectional wavelength splitter as well.

Conclusion

A bidirectional or unidirectional wavelength splitter has been proposed and investigated by an MDM structure with two asymmetric arms. According to the interference effects at the exits of the arms of the asymmetric structure, two SPP modes at the desired wavelengths will transmit through Port1 and Port2 respectively. The bidirectional wavelength splitter was with impressive performances, as the highest transmission and cross-talk isolation were ~ -0.60 and ~ 32.9 dB at 883.8 nm for Port1 and Port2, respectively, and favorable performances were also achieved for all other cases. The transmission wavelengths have been demonstrated to be linear with the lengths of the arms, which might offer flexibility to design the device. Besides, unidirectional wavelength splitter was achieved by properly adding a notch in the arm of the structure. Both SPP modes would only transmit through Port1 or Port2.

Acknowledgments The work is supported by the National Natural Science Foundation of China under Grants No. 61405039 and No. 61475037, Natural Science Foundation of Guangdong Province, China under Grant No. 2014A030310300, the State Key Lab of Optical Technologies for Micro-Engineering and Nano-Fabrication of China, the Foundation for Distinguished Young Talents in Higher Education of Guangdong, China under Grant No. 2014KQNCX066, the China Post-doctoral Science Foundation under Grant No. 2014M552173, and the Research Fund of Guangdong University of Technology under Grant No. 13ZK0387.

Compliance with Ethical Standards The content of this manuscript does not have any potential conflict of interest with anyone. This research does not involve in any human participant or animal. No part of this manuscript has been published or submitted elsewhere. Also, all the authors have given their approvals to the submission of this paper.

References

- Saito K, Tanabe T, Oyama Y (2014) THz-wave generation via difference frequency mixing in strained silicon based waveguide utilizing its second order susceptibility $\chi(2)$. *Opt Express* 22(14):16660–16668
- Yu S-P, Hood JD, Muniz JA, Martin MJ, Norte R, Hung C-L, Meenehan SM, Cohen JD, Painter O, Kimble HJ (2014) Nanowire photonic crystal waveguides for single-atom trapping and strong light-matter interactions. *Appl Phys Lett* 104(11):111103
- Rezaei M, Jalaly S, Miri M, Khavasi A, Fard AP, Mehrany K, Rashidian B (2012) A distributed circuit model for side-coupled nanoplasmonic structures with metal–insulator–metal arrangement. *IEEE J Sel Top Quant Electron* 18(6):1692–1699
- Wen KH, Hu YH, Chen L, Zhou JY, Lei L, Guo Z (2014) Design of an optical power and wavelength splitter based on subwavelength waveguides. *J Lightwave Technol* 32(17):3020–3026
- Lu H, Liu XM, Wang L, Gong Y, Mao D (2011) Ultrafast all-optical switching in nanoplasmonic waveguide with Kerr nonlinear resonator. *Opt Express* 19(4):2910–2915
- Wurtz GA, Pollard R, Zayats AV (2006) Optical bistability in nonlinear surface-plasmon polaritonic crystals. *Phys Rev Lett* 97(5):057402
- Nikolajsen T, Leosson K, Bozhevolnyi SI (2004) Surface Plasmon polariton based modulators and switches operating at telecom wavelengths. *Appl Phys Lett* 85(24):5833–5835
- Randhawa S, González MU, Renger J, Enoch S, Quidant R (2010) Design and properties of dielectric surface plasmon Bragg mirrors. *Opt Express* 18(14):14496–14510
- Bozhevolnyi SI, Volkov VS, Devaux E, Laluet JY, Ebbesen TW (2006) Channel plasmon subwavelength waveguide components including interferometers and ring resonators. *Nature* 440(7083):508–511
- Wen KH, Yan LS, Pan W, Luo B, Guo Z, Guo YH, Luo XG (2014) Electromagnetically induced transparency-like transmission in a compact side-coupled T-shaped resonator. *J Lightwave Technol* 32(9):1701–1707
- Wen KH, Yan LS, Pan W, Luo B, Guo Z, Guo YH (2013) Design of plasmonic comb-like filters using loop-based resonators. *Plasmonics* 8(2):1017–1022
- Enoch S, Quidant R, Badenes G (2004) Optical sensing based on plasmon coupling in nanoparticle arrays. *Opt Express* 12(15):3422–3427
- Park J, Kim H, Lee B (2008) High order plasmonic Bragg reflection in the metal-insulator-metal waveguide Bragg grating. *Opt Express* 16(1):413–425
- Hu FF, Yi HX, Zhou ZP (2011) Wavelength demultiplexing structure based on arrayed plasmonic slot cavities. *Opt Lett* 36(8):1500–1502
- Ma FS, Lee C (2013) Optical nanofilters based on meta-atom side-coupled plasmonics metal-insulator-metal waveguides. *J Lightwave Technol* 31(17):2876–2880
- Chen J, Li Z, Zou Y, Deng Z, Xiao J, Gong QH (2013) Coupled-resonator-induced fano resonances for plasmonic sensing with ultra-high figure of merits. *Plasmonics* 8(4):1627–1631
- Guo YH, Yan LS, Pan W, Luo B, Wen KH, Guo Z, Luo XG (2013) Characteristics of plasmonic filters with a notch located along rectangular resonators. *Plasmonics* 8(2):167–171
- Noual A, Akjouj A, Pennec Y, Gillet J-N, Djafari-Rouhani B (2009) Modeling of two-dimensional nanoscale Y-bent plasmonic waveguides with cavities for demultiplexing of the telecommunication wavelengths. *N J Phys* 11(10):103020
- Tian J, Yang R, Song L, Xue W (2014) Optical properties of a Y-splitter based on hybrid multilayer plasmonic waveguide. *IEEE J Quant Electron* 50(11):898–903
- Xu T, Zhao YH, Gan DC, Wang CT, Du CL, Luo XG (2008) Directional excitation of surface plasmons with subwavelength slits. *Appl Phys Lett* 9(10):101501
- Wen KH, Yan LS, Pan W, Luo B, Guo Z, Guo YH (2012) A four-port plasmonic quasi-circulator based on metal-insulator-metal waveguides. *Opt Express* 20(27):28025–28032

22. Babil MA, Zhou Z, Deng Q (2013) Active unidirectional propagation of surface plasmons at subwavelength slits. *Opt Express* 21(14):17066–17076
23. Pu MB, Yao N, Hu CG, Xin XC, Zhao ZY, Wang CT, Luo XG (2010) Directional coupler and nonlinear Mach-Zehnder interferometer based on metal-insulator-metal plasmonic waveguide. *Opt Express* 18(20):21030–21037
24. Raghunathan SB, Gan CH, Dijk TV, Kim BE, Schouten HF, Ubachs W, Lalanne P, Visser TD (2012) Plasmon switching: observation of dynamic surface plasmon steering by selective mode excitation in a sub-wavelength slit. *Opt Express* 20(14):15326–15335
25. Miroshnichenko AE, Kivshar YS (2013) Polarization traffic control for surface plasmons. *Science* 340(6130):283–284
26. Lin J, Mueller JB, Wang Q, Yuan G, Antoniou N, Yuan XC, Capasso F (2013) Polarization-controlled tunable directional coupling of surface plasmon polaritons. *Science* 340(6130):331–334
27. Dionne JA, Sweatlock LA, Atwater HA, Polman A (2006) Plasmon slot waveguides: towards chip-scale propagation with subwavelength-scale localization. *Phys Rev B* 73(3):035407
28. Johnson PB, Christy RW (1972) Optical constants of the noble metals. *Phys Rev B* 6(12):4370–4379